Slow Diffusion Co-Assembly as an Efficient Tool to Tune Colour Emission in Alkynyl Benzoazoles

R. Martín,[a] I. Torres-Moya,[a] B. Donoso,[a] J. R. Carrillo,[a] J. M. González-Domínguez,[b] J. Frontiñan-Rubio,[c] P. Prieto,[a,*] A. Díaz-Ortiz.[a,*]

[a] Department of Inorganic, Organic Chemistry and Biochemistry, Faculty of Science and Chemical Technologies, University of Castilla-La Mancha-IRICA, 13071 Ciudad Real, Spain

[b] Group of Carbon Nanostructures and Nanotechnology, Institute of Carbon Chemistry (ICB-CSIC), c/ Miguel Luesga Castán 4, 50018 Zaragoza, Spain

[c] Instituto Regional de Investigación Científica Aplicada, University of Castilla-La Mancha-IRICA, 13071 Ciudad Real, Spain

E-mail: Mariapilar.Prieto@uclm.es and Angel.Diaz@uclm.es

Abstract

We report here the preparation of co-assembled microcrystals by employing an easy, reproducible and cost-effective technique, namely slow diffusion. 2*H*-Benzo[*d*][1,2,3]triazole and benzo[*c*][1,2,5]thiadiazole were chosen as host and guest skeletons, respectively. Structural similarities allowed the correct co-assembly of the two structures. The co-assemblies were studied by different techniques that included Raman spectroscopy and X-ray diffraction, amongst others. The waveguiding properties and the emission colour of the doped organic microcrystals were also investigated. It was found that changes in the molar ratio of the different doping agents could tune the light emission. Fluorescence microscopy images of the co-assembled microcrystals revealed light colour changes from green to whitish, up to CIE coordinates of (0.370, 0.385). These tunable colour-active materials could be useful in the fields of optoelectronics or lab-on-a-chip for integrated optical circuits at micro-/nanoscale.

Comentario [JM1]: Here we report on

Keywords

2H-benzo[d][1,2,3]triazole, benzo[c][1,2,5]thiadiazole, co-assembly, slow diffusion, organic optical waveguide, tune colour emission

1. Introduction

Organic semiconductor micro-/nanocrystals with regular shapes have attracted a great deal of attention in recent years for many applications, such as organic field-effect transistors (OFETs),[1] organic waveguide devices,[2] and organic solid-state lasers (OSSL).[3] As a consequence, these systems are inherently ideal building blocks for key circuits in the next generation of miniaturised optoelectronic devices.[4]

Nevertheless, one of the main problems with organic molecules used in the solid state for optoelectronics is their low fluorescence quantum efficiency, which is due in part to the aggregation-induced quenching (AIE) phenomenon.[5] This problem can be solved by using co-assembled structures[6] formed by one (or more) molecule(s), one of which acts as a dopant and the other(s) as a guest. According to Förster's resonance energy transfer (FRET) mechanism,[7] the energy absorbed by the host molecules can be transferred to the guest molecule, thus leading to light emission and possibly avoiding reabsorption by the organic materials. This process has been shown to be particularly efficient in supramolecular aggregates and it is often used as a tool to tune the emission of individual particles.[8] In this way, different emission colours can be obtained in co-assembled structures by simply adjusting the molar ratio between host and dopant materials, since even small quantities of the latter dispersed in aggregates are sufficient to modify the emission spectrum and confirm an efficient energy transfer.[9]

Comentario [JM2]: Es este el acrónimo?? (no cuadra con el término) Podría ser más adecuado quizá decir "aggregation-induced quenching of emission"

Comentario [JM3]: the

The next generation of optoelectonic devices will be based on nanophotonics, a discipline in which the aim is to control and manipulate photons and/or optical energy in nanometer-scale matter. Optical waveguides are one of the essential components of these new devices.[10] Doping systems can be excellent candidates to be part of these devices. However, to date the most widely reported organic doping systems are amorphous.[11] Since the crystallinity of nanomaterials can improve their charge carrier transport and enhance the performance of optical and optoelectronic devices,[12] the development of organised co-systems is essential for optoelectronic applications. Different approaches have been employed to obtain organised co-assembled systems, including electrospinning[13] and template-assisted[8] and adsorbent-assisted physical vapour deposition (PVD) methods.[14] These methods are often tedious and require specific instrumentation. Solution-based methods are a suitable alternative to overcome these drawbacks.[15,16] Slow diffusion is an easy, reproducible and cost-effective technique that can produce organised structures without specialised equipment.

It is well known that organic white-light emission (WLE) materials are essential for full-colour displays and the backlight of portable display devices.[17] For this reason, modulation of colour emission is a crucial factor in current research. Several supramolecular approaches have been reported for WLE generation by self-assembly[18] or gelation[19] of molecular building blocks that emit the three primary colours, i.e., red, green, and blue.

In the last few years our ongoing research line has been based on the design and preparation of new organic optical waveguides based on azole and benzoazole derivatives.[20] In this respect, we recently described the doping of a 2*H*-benzo[*d*][1,2,3]triazole derivative with graphene. This strategy allowed us to modulate the emission colour of the graphene-modified aggregate.[21]

In the work described here we studied different co-assembled structures from derivatives **1** and **2** (Figure 1) previously prepared by our research group by means of Sonogashira C–C cross-coupling reactions between the dibromobenzotriazole or dibromobenzothiadiazole derivative

and the corresponding arylacetylene.[20c-e] The 2*H*-benzo[*d*][1,2,3]triazole core was selected as the donor host skeleton due to its exceptional ability to form well-defined rod-like self-assembled aggregates.[20c] This core is able to emit in the blue and near green regions. Doping of the benzotriazole **1** with the green and red dye derivatives of benzo[*c*][1,2,5]thiadiazole **2** as guest molecules[21] allows the light emission to be successfully tuned from the green to the orange region and the colour can be adjusted by simply modifying the molar ratio. The similar structures of the host and guest molecules ensure the confinement and proximity of donor and acceptor molecules in co-assembled microstructures, thus resulting in efficient FRET in the donor-acceptor system.[7]

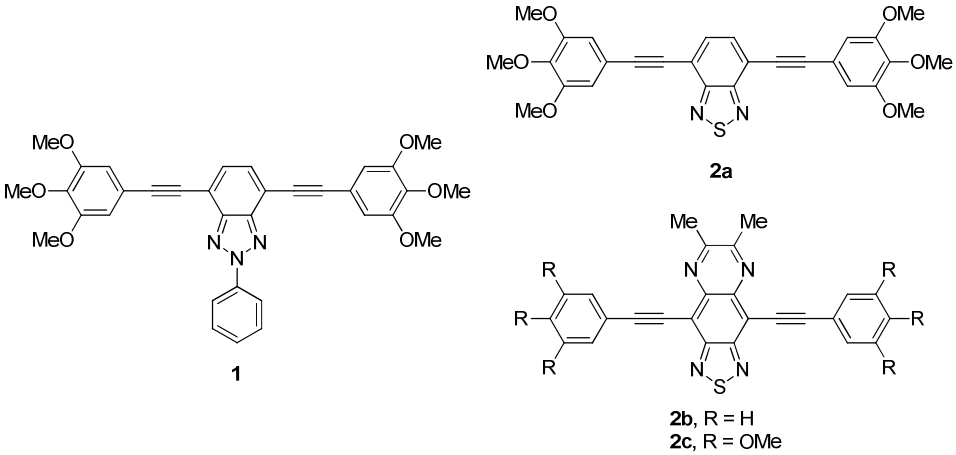

Figure 1. Structures of derivatives **1** and **2** used as host and guest materials, respectively.

2. Results and Discussion

2.1 Self-assembly behaviour

Organised supramolecular co-assembled structures were obtained by the slow diffusion technique. Thus, 10^{-3} M stock solutions of **1** and **2** were prepared in THF. Five different doping ratios **1**:**2** were chosen as follows: 1:0.1; 1:0.3; 1:1; 1:3; 1:9. The specific compositions **1**:**2** were obtained by mixing the appropriate volumes to form 1 mL of THF solution. An open sample vial containing the mixed solutions was gently placed in a vessel containing MeOH as the poor solvent and the system was sealed. After several days of slow diffusion, a uniform precipitate was observed in the inner vial. It is interesting to note that co-assembled structures are only formed up to 1:0.3 molar ratios. In order to avoid false luminescence emission signals arising from remaining solutions of doping agents that could coat the co-assembled crystals, the crystals were washed with two different solvents: hexane and methanol. Despite the fact that both solvents removed the coating products, methanol, being a more polar solvent, could

dissolve some of the crystal and it was found that hexane was the best option to ensure the integrity of the crystal (compare Figures 2 and S1–S2).

Visual changes confirmed that a co-assembly process had taken place and dye leakage was not observed during the preparation process. Homogeneous crystals were formed with a different colour from the pure host. Whereas pure **1** forms clear yellow crystals with an intense yellow emission under 365 nm (Figure 2A,B), the colour of doped **2a** and **2b** crystals were clear orange (Figure 2I,J) and red (Figure 2K,L), respectively, due to the incorporation of the doping compound into the host structure. More strikingly, **2c**-doped crystals were dark brown when the co-assembly process was completed (Figure 2M,N), thus providing evidence that all of the acceptor dyes **2** had been doped into the organic microcrystals of **1**. It is worth noting that in cases where the slow diffusion conditions were not satisfactory (solvent, temperature, proportions, time etc.), co-assembled crystals did not form and separate precipitates of pure host and guest molecules were observed (Figure S3). In order to ascertain whether co-assembled structures were formed in the slow diffusion process, 1 mL of a pure solution of **2a** and **2c** was added to pure microcrystals of **1**. After several days neither visual changes nor different emission were observed in the crystals of **1** (Figure S4). Thus, the co-assembly process only takes place if slow diffusion is carried out.

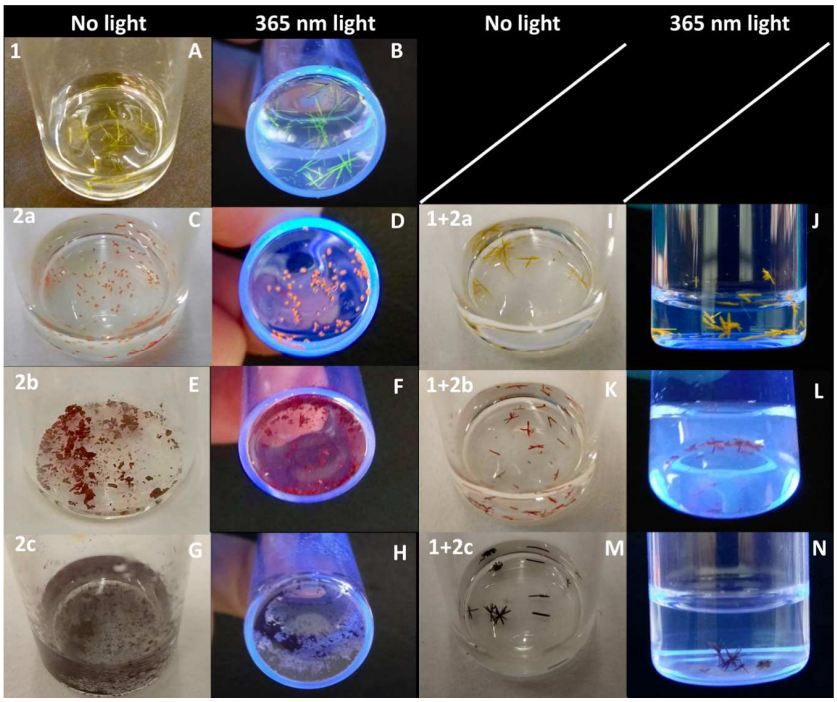

Figure 2. Pure self-assembled crystals of **1** (A,B), **2a** (C,D), **2b** (E,F) and **2c** (G,H) under natural light and irradiated at 365 nm. Pictures of the co-assembled structures (I–N) with the doping agents represented. All structures were removed from their original solution and washed with hexane in order to avoid false emission signals.

The resulting morphologies of the co-assembled crystals were visualised by scanning electron microscopy (SEM) on glass substrates (Figure 3). Pure benzotriazole **1** produced well-defined rod-like aggregates that were hundreds of micrometres in length by slow diffusion using chloroform ($CHCl_3$) as the good solvent and acetonitrile (CH_3CN) as the poor solvent.[20c] However, the use of THF/MeOH as solvents in the slow diffusion process gave ultra-long self-assembled needle-like crystals that were several millimetres in length – a process that could facilitate their use in optoelectronic devices (Figure S5).

It was found that the percentage of doping agents must be less than 25% in order to favour crystal growth by the slow diffusion technique. In general, when compared with pure microcrystals of **1**, the co-assembled structures had very few morphological differences, which indicates that the host (**1**) has a greater tendency to aggregate than the guest (**2**) and the acceptor organic molecules will not affect the macroscopic crystallinity of the as-prepared organic microstructures (Figure 3). In the case of **2c** only a 1:0.1 host:guest ratio afforded co-assembled structures.

In general, co-assembled structures are more planar than pure self-assembled **1** (Figure 3E-I *vs.* A) and this is especially noteworthy in the case of **2c**-doped crystals (Figure 3I).

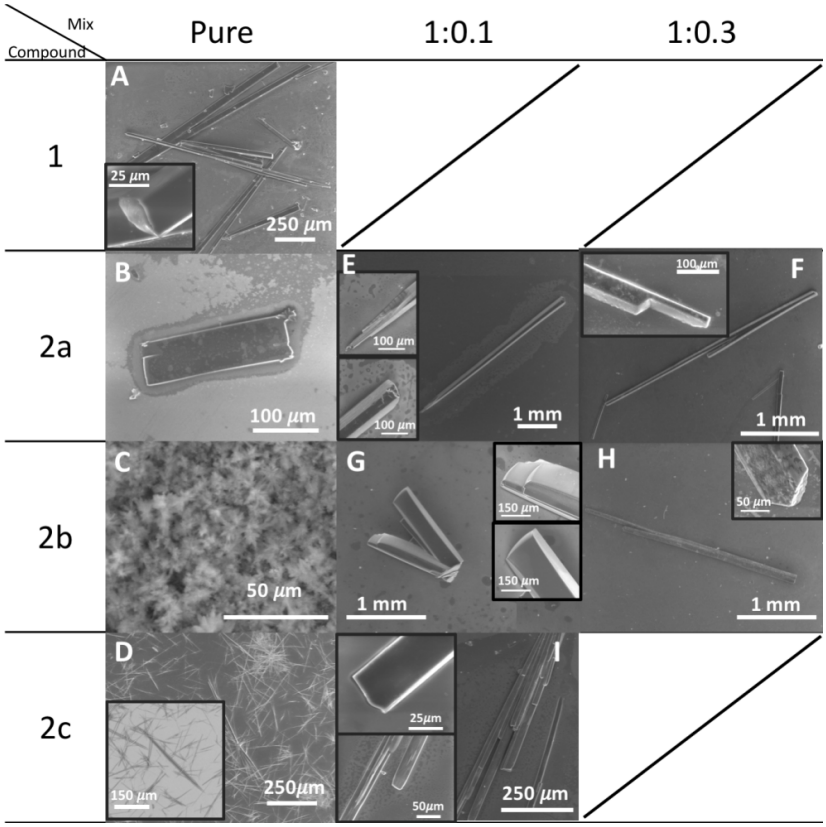

Figure 3. SEM images of pure self-assembled **1** and **2**, and the resulting morphologies of 1:0.1 and 1:0.3 molar ratio co-assembled structures obtained by slow diffusion of MeOH vapour into dilute THF solutions.

NMR spectroscopy was employed in an effort to confirm further that the co-assembly process of both derivatives occurred effectively. Hexane-washed co-assembled crystals **1**:**2a** (1:0.3) were dissolved in 600 μL of $CDCl_3$. The proton signals of both **1** and **2** were observed in the NMR spectra and this confirmed that the two molecules coexist in the crystal (Figure S6). Furthermore, other spectroscopic techniques were applied to obtain information about the co-assembled system and these are discussed in the following sections.

2.2 Raman analysis

A Raman spectroscopy study was performed on selected samples. After an initial screening it was only possible to carry out Raman spectroscopy on compound **2c**. The high fluorescence of derivatives **2a** and **2b** precluded their study by this technique. The identification of each component was made on the basis of the intensity of a specific peak. The peak at 1416 cm^{-1} was chosen for compound **1** and for compound **2c** the peak at 1334 cm^{-1} was selected as a representative feature.

Representative Raman spectra for organic compounds **1** and **2c** are shown in Figure 4. Given the vibrational nature of Raman spectroscopy, the different peaks can be ascribed to specific vibrations according to the molecular structure. Compound **1** presented the alkyne stretching band at 2200 cm^{-1} as the most prominent feature. Furthermore, aromatic ring vibrations also had a strong presence in the spectrum, namely the N=N and C=C stretchings at 1416 cm^{-1} and 1572 cm^{-1}, respectively. Compound **2c** had a Raman profile that was similar to that of the host (**1**) in terms of the alkyne and aromatic C=C bands, while other bands related to other carbon bonds, such as C–C stretching (1283 cm^{-1}) and methyl bending (1334 and 1481 cm^{-1}), were observed.

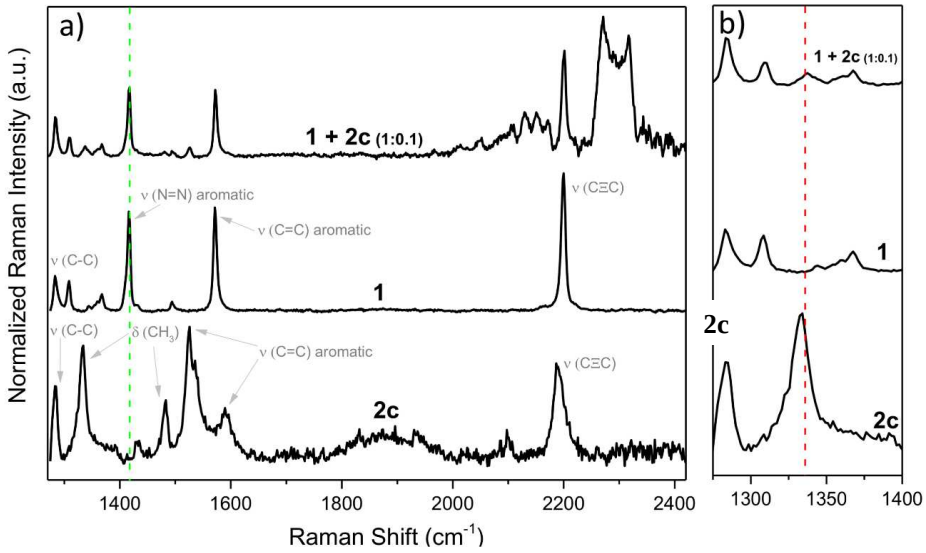

Figure 4. a) Raman spectra (532 nm laser) of compounds **1**, **2c**, and the mixture of **1:2c** (1:0.1 ratio). The assignments of the main vibrational bands are depicted. Dashed vertical lines indicate the peaks used in the two-dimensional mapping to identify each compound: green for compound **1** and red for compound **2c**, with interference not observed between the two sets of signals. b) Inset of the lower part of the spectra, for the sake of clarity, showing the selected 1334 cm^{-1} band belonging to compound **2c**.

In the two-dimensional Raman mappings (Figures 5, S1 and S2) specific colours were assigned to each peak (red for 1334 cm^{-1} and green for 1416 cm^{-1}) and these were plotted simultaneously, using Wire 4.4 software, according to the intensity of the respective peaks. This process allowed us to ascertain the relative disposition of each compound in the mixtures.

In general terms, it can be seen how the co-assembled crystals **1**:**2c** (1:0.1) present an uneven distribution of the two components within the crystal. Thus, by Raman spectroscopy it was determined that these crystals are formed by a matrix of aggregated **1** with small clusters of **2c** randomly scattered across the structure (Figure 5). This trend was still visible after the crystals were washed with hexane (Figure 5 and S1). However, a different situation was observed when the crystals were washed with methanol (Figure S2). In this case, the distribution of **2c** islands within **1** became unclear and the resulting colour mapping suggested that a merging of the two compounds had taken place. This finding is in good agreement with the experimental observations that methanol is able to partially dissolve the crystalline structure of this mixture.

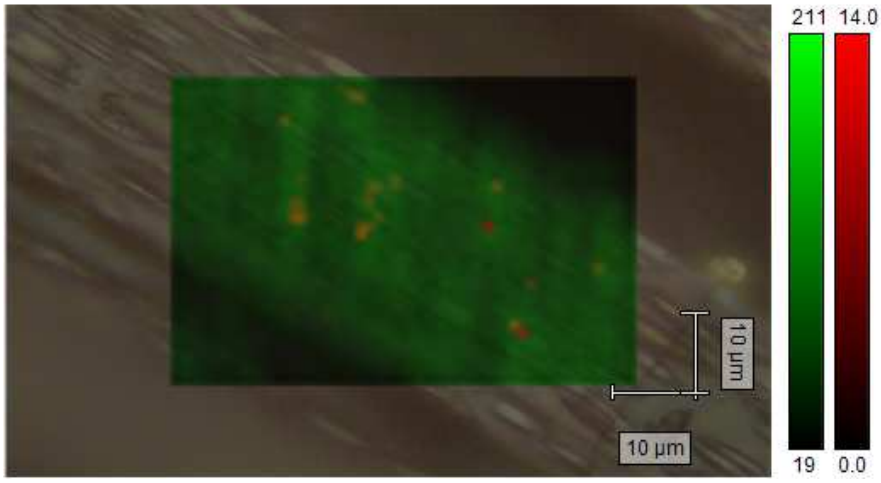

Figure 5. 2D Raman mapping (532 nm laser) of a selected region of a co-assembled crystal **1:2c** (1:0.1) from characteristic bands of **1** (in green) and **2c** (in red). Numbers in the coloured bars are arbitrary.

2.3 X-ray analysis

Comentario [JM4]: diffraction

The crystal structures of the binary nanomaterials were studied by X-ray diffraction (XRD) and the profiles of the pure and doped nanowires were obtained. For the different compounds the diffraction pattern of the binary nanowires shows diffraction peaks for the host and guest compounds. This indicates that **1** is also crystalline in the doped nanomaterials but the formation of a co-crystal or superlattice-type composite crystal did not occur (Figures 6, S7 and S8). Furthermore, a significant displacement of the peak at $2\theta = 15.00^{o}$ of the structure of **1** can be observed (which corresponds to an interplanar spacing of 5.90 Å) to $2\theta = 14.68^{o}$ (interplanar spacing of 6.03 Å) in the doped structure. This may indicate that for molecules of **1** the interplanar spacing along the b-axis increases in order to accommodate molecules of **2a**. This peak displacement appears in the three doped nanowires, probably due to the similar structures of the doping agents.

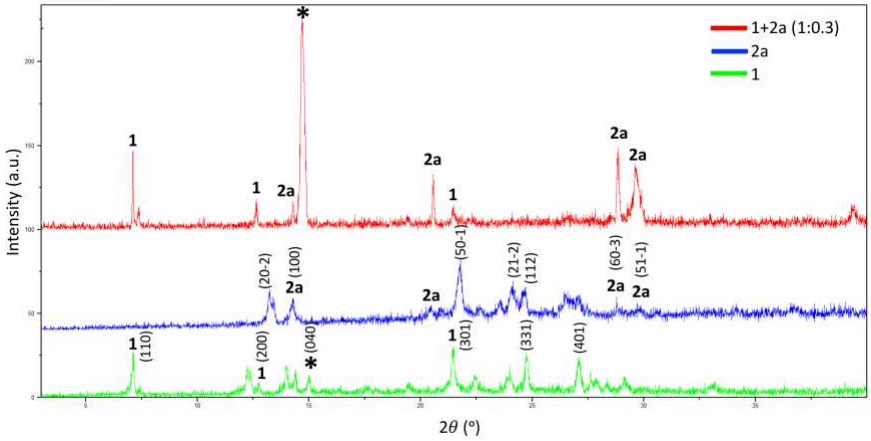

Figure 6. XRD patterns of the pure compounds **1** (green) and **2a** (blue), and the doped organic microcrystal with **1**:**2a** (1:0.3) (red). The stars indicate the diffraction peak of 2θ = 14.68º for **1**, which exhibits a significant displacement in the doped structures. The numbers '1' and '2a' indicate the diffraction peaks of the pure structures **1** and **2a**, respectively. Crystal planes were assigned from the X-ray structures of the pure compounds.

2.4 Photophysical features

The optical spectra of compounds **1** and **2** were experimentally measured in tetrahydrofuran (THF) (Figure 7). Only a slight overlap between the emission band of **1** and the absorption band of **2a** can be seen in Figure 7A. However, it should be noted that the emission spectrum of **1** shows a good overlap with the absorption spectra of **2b** and **2c** in the wavelength range 450–600 nm (Figures 7B and 7C, respectively), which may result in efficient energy transfer from the host **1** to the guest **2** in the doped system. Doping organic derivatives **2** as acceptors into a donor host matrix of benzotriazole **1** ensures confinement and proximity of the two molecules within self-assembled microstructures, thus resulting in efficient FRET in the donor-acceptor system.[15,22]

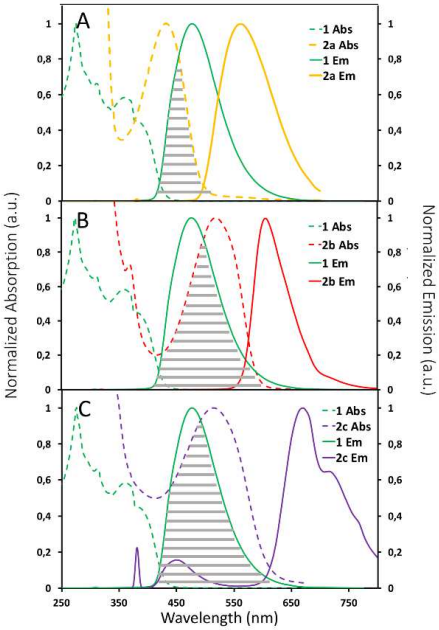

Figure 7. Absorption and emission spectra of pure **1** (green), **2a** (orange), **2b** (red) and **2c** (purple). Overlap between the absorption spectrum of **1** and fluorescence spectrum of **2** is denoted with grey lines. All spectra were measured in THF solution. PL spectra were measured after excitation at the maximum absorption peak of the corresponding compounds. Absorption spectra of compounds **2** were normalised to its ICT band.

2.5 Optical waveguiding properties

Considering the previously reported results on the optical waveguiding features of the related pure compounds **1**[20c] and **2a**,[20e] we investigated the propagation of light in the aggregates formed from co-assembled structures. These studies were carried out by fluorescence microscopy. Pure **1** aggregates exhibited blue and green bright luminescence spots at the opposite ends and a relatively weak emission from the body when it was irradiated at one end (Figure S9).

The co-structures discussed above were irradiated with a laser beam at different λ values and the resulting fluorescence images were recorded with a camera (Figure 8). When benzotriazole **1** was doped with 10% of **2a** (1:0.1 molar ratio) only green light was propagated through the structure (Figure 8A). Interestingly, when the proportion of the doping agent **2a** was 25% (doping ratio 1:0.3), the structure was also able to propagate red light (Figure 8B). This finding provides evidence that changes in the doping agent ratio can modify the propagated light. A similar result has been reported previously in the literature.[17d]

Co-assembled structures containing compound **2c** only propagated red light when they were irradiated at one end (Figure 8D). This characteristic could due to the large overlap between the emission band of **1** and the absorption band of **2c** at 430–570 nm (Figure 7C), which would

favour the reabsorption of light. When the host structure was doped with **2b** both green and red light were propagated through the structure (Figure 8C). A lower level of overlap between the emission band of **1** and the absorption band of **2b** is observed in the PL spectra of pure compounds, which indicates that the reabsorption process is less effective (Figure 7B). These results show that the presence of different doping agents can modify the emission colour of the molecular aggregate with waveguide properties. In this specific case, the dopant dyes cause a bathochromic shift in the emission colour of **1**, which changes from blue and green emission to green-red or red emission with the appropriate ratio of doping agent.

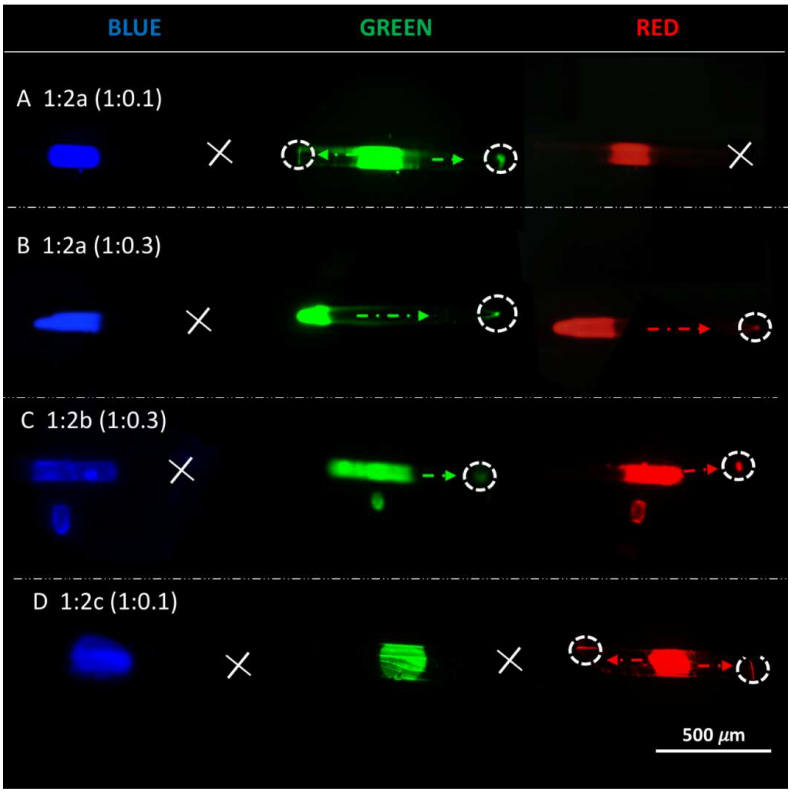

Figure 8. Fluorescence images of the co-assembled aggregates **1**:**2a** 1:0.1 molar ratio (A), 1:0.3 molar ratio (B), **1**:**2b** 1:0.3 molar ratio (C), and **1**:**2c** 1:0.1 molar ratio (D) obtained by irradiating a portion of the aggregate at 320–380 nm (blue), 450–490 nm (green), and 515–565 nm (red). The propagated light at the end of the crystal is shown with a white dashed circle and the direction of the light with a dashed arrow.

2.6 White light-emission

It is well known that a mixture of blue, green and red chromophores can afford structures that emit white light.[17] Bearing this in mind, it was decided to carry out a photophysical study on mixtures of compound **1** with different compositions of the three doping agents. The fluorescence emission spectra of solutions are shown in Figure 9.

In mixtures with **2a** only one broad emission band can be observed due to the low Stokes shift (79 nm) between the emission bands of **1** and **2a** (Figure 7A and 9A). Mixtures made with derivative **2c** showed very poor emission in solution (Photoluminescence Quantum Yield, PLQY = 0.08%),[23] so an emission band corresponding to this compound was not observed in the fluorescence spectra of the mixture (Figure 9C) and only a decrease in the intensity of the band due to **1** was observed as its molar ratio decreased.

In the case of **2b**, for which the PLQY was 67%[23] and where the Stokes shift between the emission bands of **1** and **2b** was 127 nm, the mixed solution of compounds showed two dominant emission bands located at around 500 and 600 nm. These bands can be attributed to molecules of compound **1** and the dopant **2b**, respectively (Figure 9B).

The emission wavelengths of both **1** and **2** did not show any obvious differences from those of the monomers, so the emission colour of the as-prepared binary 1D microstructures was mainly dependent on the doping ratio. Luminescence photographs of the solutions upon increasing the dopant ratio with excitation 365 nm are shown in Figure 9. The colours of the solutions are consistent with the corresponding emission spectra. In general, the presence of higher levels of doping agent (**2**) gave rise to lower emission of the host (**1**).

It is worth noting the presence of a broad emission band (450–700 nm) and a visual white emission of the solution **1**:**2b** when the doping ratio was 1:0.3 (Figure 9B), which hints at a possible white emission in the solid state for the crystal with this doping ratio.

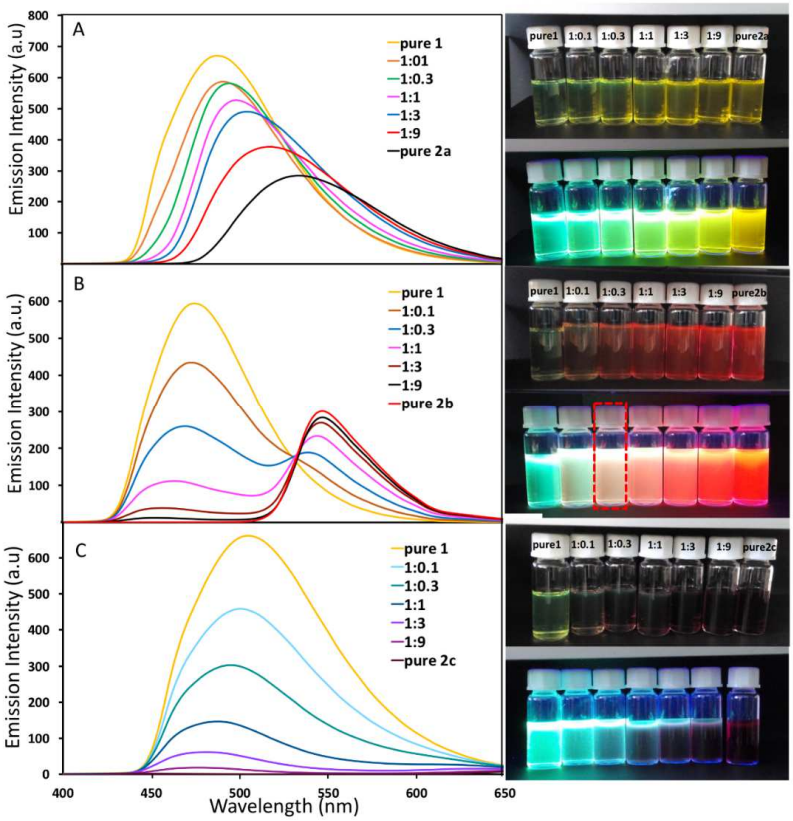

Figure 9. Fluorescence spectra and luminescence photographs of THF solutions of **1** upon increasing the dopant ratio of **2a** (A), **2b** (B) and **2c** (C). Luminescence photographs were taken under natural light (above) and 365 nm light (below).

The optical properties of the co-assembled structures with different doping ratios were also investigated and the PL spectra of the as-prepared microcrystals are shown in Figure 10c.

The confocal microscopy images (Figure 10a) of the co-assembled microrods reveal only slight colour changes from green to whitish upon increasing the molar doping ratio – an observation that indicates the successful modulation of the light emission of the organic microcrystals. The uniform emission colour of each single wire reveals that the guest molecules of **2** are dispersed very uniformly in the matrix **1**, which is in good agreement with Raman spectroscopy data (Figure 5). The CIE coordinates of these pure and co-assembled structures are presented in Figure 10b. The CIE coordinates (0.370, 0.385) of the microcrystals with a **2b** doping ratio of 1:0.3 correspond to the white-emissive region in the CIE chromaticity diagram.

Doping ratios of 1:0.2 and 1:0.5 were also tested with **2b** as the doping agent (Figures S10 and S11). It was found that a 1:0.2 ratio was not sufficient to achieve white emission and pale-yellow crystals were obtained. In contrast, a 1:0.5 ratio gave green-yellow crystals.

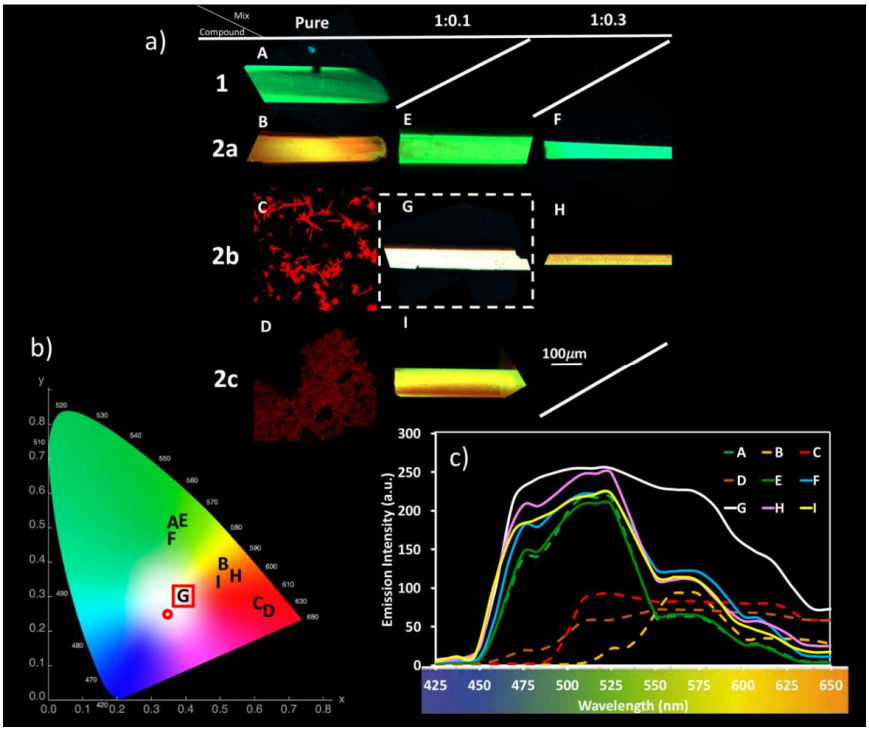

Figure 10. a) Fluorescence microscopy images of the microcrystals containing different doping ratios of **2** upon excitation at 425–650 nm; b) The emission colours corresponding to the organic microcrystals shown in (a) the CIE chromaticity diagram. The white emission colour is marked as a red circle in the CIE chromaticity diagram; c) Emission spectra of the microcrystals shown in (a) deposited onto quartz wafers.

3. Conclusions

The 2*H*-benzo[*d*][1,2,3]triazole core has been employed as a host skeleton to prepare well-defined co-assembled microcrystals. The exceptional ability to form well-defined rod-like self-assembled aggregates and the blue and near-green emission of this compound has been successfully combined with the intense green and red emissions of benzo[*c*][1,2,5]thiadiazole guest molecules.

The co-assembled microcrystals were obtained by the slow diffusion technique, which is an easy, reproducible and cost-effective approach. Five doping ratios were tested and it was found that the percentage of doping agent must be less than 25% in order to favour crystal growth.

Comentario [JM5]: lower

All of the co-assembled microcrystals prepared in this study showed impressive visual colour changes from the pure host, thus confirming that a co-assembly process had successfully taken place. The arrangement of the co-assembled structures was analysed by different spectroscopic and microscopic techniques.

SEM analysis did not indicate any significant morphological differences in the structures of the co-assembled microcrystals when compared to pure **1**. This finding indicates that the host material drives the formation of the organised co-assembled structures.

X-ray diffraction analysis revealed that the crystallinity of the host material (**1**) remains unaltered when the guest material (**2**) is incorporated, and a co-crystal or superlattice-type composite crystal is therefore not formed. However, it was found that molecules of **1** increase their interplanar spacing along the b-axis in order to accommodate molecules **2**.

Evidence for a randomly scattered distribution of the guest molecule (**2c**) in the matrix structure of the host molecule (**1**) was provided by Raman spectroscopy.

The co-assembled microcrystals can act as optical organic waveguides and the propagation of the light in the resulting aggregates could be modulated by altering both the doping agent and the doping ratio. The light reabsorption process must be avoided in order to allow propagation of light with a different wavelength along the co-assembled microcrystals.

The emission spectra of the mixed solution of **1**:**2b** with a 1:0.3 molar doping ratio revealed the presence of a broad emission band (450–700 nm) and a visible white emission from the solution. The CIE coordinates of this solid co-assembled aggregate were (0.370, 0.385). Colour changes in the light from green to orange were observed for the rest of co-assembled microcrystals and this indicates successful modulation of the light emission of the organic microcrystals.

Comentario [JM6]: Para que las conclusiones no queden meramente descriptivas y se vea la proyección futura de estos resultados, creo que vendría bien alguna frase conclusiva del tipo: “the results presenteed herein offer a versatile approach towards affordable white emissive materials for future application in optoelectronic devices” (o quizá algo más específico si queréis)

4. Experimental details

Compounds **1** and **2a-c** were prepared according to experimental procedures described by our research group.[20e,c, 23]

SEM images were obtained on a JEOL JSM 6335F microscope working at 15 kV. The samples for SEM imaging were prepared by slow diffusion by mixing the appropriate proportions of compounds **1** and **2**. The corresponding solids were washed with hexane and deposited onto a glass substrate, with the remaining solvent evaporated at room temperature.

Raman spectra were recorded on a Renishaw inVia™ microspectrophotometer using a 532 nm wavelength laser (85 mW effective output power), with the system coupled to an optical microscope. The sample preparation for Raman measurements was performed by drop casting a THF solution onto a clean piece of SiO_2/Si wafer (WRS Materials) and leaving the solvent to evaporate in the open air. Point-based spectra were collected using the 100× objective (N.A. = 0.85), 0.1% of the maximum laser power, and 1 second of exposure time at each pulse, in order to avoid thermal damage to the sample and interference by fluorescent emission. Each spectrum was baseline-corrected and normalised (to its own highest intensity band) using the Renishaw Wire 4.4 software tool. As regards two-dimensional mapping, a line-based laser option was used (streamline). The experimental conditions were set up in the range of 0.1–1 seconds

Comentario [JM7]: to

Comentario [JM8]: mappings

exposure time and 0.05–0.1% of the maximum laser power. The probed areas were approximately 20–25 mm^2.

The XRD patterns were obtained on a PANalytical X'Pert X-ray diffractometer with Cu-Kα radiation (λ = 1.54056 Å). For this study the optimal parameters were run with an increment size of 0.01° and an increment scan time of 1 second over a scan range of 3–40 2θ.

Powdery crystals of pure and doped compounds were deposited on a Si zero diffraction plate. This kind of sample holder has no background noise from 20 to 120 degrees and ensures that diffraction peaks are obtained from the sample.

Crystal planes of **1** and **2a** were assigned for comparison with the corresponding XRD pattern simulated from their X-ray structures.[20b,c,e, 21]

UV-vis spectra were recorded on a Jasco V-530 spectrophotometer. Fluorescence spectra were recorded on a Jasco FP-750 spectrophotometer. In both cases standard quartz cells (1 cm width) were used. Spectra were recorded at room temperature using solvents of spectroscopic grade.

Fluorescence images for waveguide behaviour were recorded on a ZEISS Axioplan-2 fluorescence microscope with a mercury lamp capable of excitation at any wavelength. However, a series of filters was used to select the excitation wavelength and absorption. These correspond to wavelengths in the blue (λexc = 320–380 nm, λem = 410–510 nm), green (λexc = 450–490 nm, λem = 515–565 nm) or red (λexc = 475–495 nm, λem = 520–570 nm). This microscope was fitted with a shutter that allowed the light to be focused on the desired part of the crystal.

A Zeiss LSM 800 confocal microscope (Zeiss, Jenna, Germany) with a 10× objective (Plan-Apochromat 10×/0.45 M27) equipped with the ZEN imaging software was used to collect RGB and spectral images of the microcrystals containing different doping ratios of **2**. RGB images were obtained using three diode lasers (405, 488 and 561) for blue, green and red fluorescence. Spectral imaging was carried out with laser excitation in the 425–650 nm emission range. A set of 26 images was obtained, with each image acquired with a separate narrow bandwidth of 8 μM, thus representing the complete spectral distribution of the fluorescence signals.

Acknowledgements

This work has been financially supported by JCCM-FEDER (project SBPLY/17/180501/000189) and MINECO of Spain (projects CTQ2017-88158-R and CTQ2017-84825-R). R. Martín and B. Donoso are indebted to MEC for a FPU studentship. We thank Mr. Carlos Rivera for his help in the X-ray analysis.

References

1. a) Shin H, Kumar A, Chao H, Yang D, Palai AK, Pyo S. Laterally-Stacked, solution-processed organic microcrystal with ambipolar charge transport behavior. ACS Appl Mater Interfaces

2014;6:17804-14. http://dx.doi.org/10.1021/am5044505; b) Kabe R, Nakanotani H, Sakanoure T, Yahiro M, Adachi C. Effect of molecular morphology on amplified spontaneous emission of bis-styrylbenzene derivatives. Adv Mater 2009;21:4034-8. http://dx.doi.org/10.1002/adma.200803588; c) Mas-Torrent M, Hadley P, Bromley ST, Ribas X, Tarres J, Mas M, Molins E, Veciana J, Rovira C. Correlation between crystal structure and mobility in organic field-effect transistors based on single crystals of tetrathiafulvalene derivatives. J Am Chem Soc 2004;126:8546-53. http://dx.doi.org/10.1021/ja048342i; d) Wang Y, Guo H, Ling S, Arrechea-Marcos I, Wang Y, Lopez Navarrete JT, Ponce Ortiz R, Guo X. Ladder-type heteroarenes: up to 15 rings with five imide groups. Angew Chem Int Ed 2017;56:9924-9. http://dx.doi.org/10.1002/anie.201702225.

2. a) Chandrasekar R. Organic photonics: prospective nano/micro scale passive organic optical waveguides obtained from π-conjugated ligand molecules. Phys Chem Chem Phys 2014;16:7173-83. http://dx.doi.org/10.1039/C3CP54994A; b) Gu X, Yao J, Zhang G, Yan Y, Zhang C, Peng Q, Liao Q, Wu Y, Xu Z, Zhao Y, Fu H, Zhang D. Influence of alkyl chain lengths on the properties of iridium(III)-based piezochromic luminescent dyes with triazole-pyridine type ancillary ligands. Adv Funct Mater 2012;22:4862-72. http://dx.doi.org/10.1016/j.dyepig.2013.08.015; c) Guo Z-H, Lei T, Jin Z-X, Wang J-Y, Pei J. T-shaped donor–acceptor lolecules for Low-loss red-emission optical waveguide. Org Lett 2013;15:3530-3. http://dx.doi.org/10.1021/ol4012025; d) Li Q, Jia Y, Dai L, Yang Y, Li J. Controlled rod nanostructured assembly of diphenylalanine and their optical waveguide properties. ACS Nano 2015;9:2689-95. http://dx.doi.org/10.1021/acsnano.5b00623; e) Wang X, Han Y, Liu Y, Zou G, Gao Z, Wang F. Cooperative supramolecular polymerization of fluorescent platinum acetylides for optical waveguide applications. Angew Chem Int Ed 2017;56:12466-70. http://dx.doi.org/10.1002/anie.201704294; h) Li Y, Ma Z, Li A, Xu W, Wang Y, Jiang H, Wang K, Zhao Y, Jia X. A single crystal with multiple functions of optical waveguide, aggregation-induced emission, and mechanochromism. ACS Appl Mater Interfaces 2017;9:8910-8. http://dx.doi.org/10.1021/acsami.7b00195.

3. a) Wang X, Li H, Wu Y, Fu H. Tunable morphology of the self-assembled organic microcrystals for the efficient laser optical resonator by molecular modulation. J Am Chem Soc 2014;136:16602-8. http://dx.doi.org/10.1021/ja5088503; b) Wang X, Liao Q, Kong Q, Zhang Y, Xu Z, Lu X, Fu H. Whispering-gallery-mode microlaser based on self-assembled organic single-crystalline hexagonal microdisks. Angew Chem Int Ed 2014;53:5863-7. http://dx.doi.org/10.1002/anie.201310659; c) Wang X, Liao Q, Xu Z, Wu Y, Wei L, Lu X, Fu H. Exciton-polaritons with size-tunable coupling strengths in self-assembled organic microresonators. ACS Photonics 2014;1:413-20. http://dx.doi.org/10.1021/ph400160v.

4. a) Zhao YS, Fu H, Hu F, Peng A, Yao. Multicolor emission from ordered assemblies of organic 1D nanomaterials. J. Adv Mater 2007;19:3554-8. http://dx.doi.org/10.1002/adma.200701513; b) Ong BS, Wu YL, Liu P, Gardner S. High-performance semiconducting polythiophenes for organic thin-film transistors. J Am Chem Soc 2004;126:3378-9. http://dx.doi.org/10.1021/ja039772w; c) Wang ZL. Nanobelts, Nanowires, and nanodiskettes of semiconducting oxides-from materials to nanodevices. Adv Mater 2003;15:432-6. http://dx.doi.org/10.1002/adma.200390100; d) Law M, Greene LE, Johnson JC, Saykally R, Yang P. Nanowire dye-sensitized solar cells. Nat Mater 2005;4:455-9. http://dx.doi.org/10.1038/nmat1387; e) Liu H, Li Y, Jiang L, Luo H, Xiao S, Fang H, Li H, Zhu D, Yu D, Xu J, Xiang B. Imaging as-grown [60]Fullerene nanotubes by template technique. J Am Chem Soc 2002;124:13370-1. http://dx.doi.org/10.1021/ja0280527; f) Li X, Gu H, Chen K, Song L, Hao Q. STorus: A new topology for optical network-on-chip. Optical Switching and Networking (OSN) 2016;22:77-85. http://dx.doi.org/10.1016/j.osn.2016.04.004.

5. a) Birks JB. Photophysics of Aromatic Molecules; Wiley: New York, 1970; b) Yuang Z, Liu P, Chen S, Lam JWY, Wang Z, Liu Y, Kwok HS, Ma Y, Tang BZ. Changing the behavior of chromophores from aggregation-caused quenching to aggregation-induced emission: development of highly efficient light emitters in the solid state. Adv Matter 2010;22:2159-63. http://dx.doi.org/10.1002/adma.200904056; c) Huang Y, Xing J, Gong Q, Chen L-C, Liu G, Yao C, Wang Z, Zhang H-L, Chen Z, Zhang Q. Reducing aggregation caused quenching effect through co-assembly of PAH chromophores and molecular barriers Nature Commun 2019;10:art. nº 169. http://dx.doi.org/10.1038/s41467-018-08092-y.

6. a) Mendez H, Heimel G, Optiz A, Sauer K, Barjowski P, Oehzelt M, Soeda J, Okamoto T, Takeya J, Arlin JB, Balandier JY, Geerts Y, Koch N, Salzmann I. Doping of organic semiconductors: impact of dopant strength and electronic coupling. Angew Chem Int Ed 2013;52:7751-55. http://dx.doi.org/10.1002/anie.201302396; b) Huang D, Wang C, Zou Y, Zhen

X, Zang Y, Shen H, Gao X, Yi Y, Xu W, Di C-A, Zhu D. Bismuth interfacial doping of organic small molecules for high performance n-type thermoelectric materials. Angew Chem 2016;128:10830-3. http://dx.doi.org/10.1002/ange.201604478.

7. a) Förster, T. Intermolecular energy migration and fluorescence. Ann Phys 1948;2:55–75. http://dx.doi.org/10.1002/andp.19484370105; b) Hohng S, Lee J, Lee S. Single-Molecule Three-Color FRET with Both Negligible Spectral Overlap and Long Observation Time. PLOS ONE 2010;5:e12270. http://dx.doi.org/10.1371/journal.pone.0012270; c) Jones GA, Bradshaw DS. Resonance energy transfer: From fundamental theory to recent applications. Frontiers in Physics. 2019;7:100. http://dx.doi.org/10.3389/fphy.2019.00100.
8. Tseng K-P, Tsai Y-T, Shyue J-J, Raffy G, del Guerzo A, Wong K-T, Bassini DM. Emissive nanotubes from templated self-assembly of small molecules. Chem Phys Lett 2017;683:43-8. http://dx.doi.org/10.1016/j.cplett.2017.04.005.
9. a) Xu Z, Liao Q, Shi X, Li H, Zhang H, Fu H. Full-color tunable organic nanoparticles with FRET-assisted enhanced two-photon excited fluorescence for bio-imaging. J Mater Chem B 2013;1:6035-41. http://dx.doi.org/10.1039/C3TB20841A; b) Fang H-H, Lu S-Y, Wang L, Ding R, Wang H-Y, Feng J, Chen Q-D, Sun H-B. Preparation and time-resolved fluorescence study of RGB organic crystals. Org Electron 2013;14:389-95. http://dx.doi.org/10.1016/j.orgel.2012.10.028.
10. a) Zhang W, Zhao YS. Organic nanophotonic materials: the relationship between excited-state processes and photonic performances. Chem Commun 2016;52:8906-17. http://dx.doi.org/10.1039/C6CC00018E; b) Zhang C, Zhou C-L, Zhao Y, Dong C-H, Wei C, Wang H, Liu Y, Guo G-C, Yao J, Zhao YS. Organic printed photonics: From microring lasers to integrated circuits. Science Adv 2015;1:e1500257. http://dx.doi.org/10.1126/sciadv.1500257; c) Zhao G, Dong H, Liao Q, Jiang J, Luo Y, Fu H, Hu W. Organic field-effect optical waveguides. Nature Commun 2018;9:art nº 4790. http://dx.doi.org/10.1038/s41467-018-07269-9.
11. a) Peng A, Xiao D, Ma Y, Yang W, Yao J. Tunable emission from doped 1,3,5-triphenyl-2-pyrazoline organic nanoparticles. Adv Mater 2005;17:2070-3. http://dx.doi.org/10.1002/adma.200401989; b) Tang CW, van Slyke SA, Chen CH. Electroluminescence of doped organic thin films. J Appl Phys 1989;65:3610-16. http://dx.doi.org/10.1063/1.343409; c) Kido J, Kimura K, Nagai K. Multilayer white light-emitting organic electroluminescent device. Science 1995;267:1332-34. http://dx.doi.org/10.1126/science.267.5202.1332.
12. a) Zhao YS, Di C, Yang W, Yu G, Liu Y, Yao. Photoluminescence and electroluminescence from tris(8-hydroxyquinoline)aluminum nanowires prepared by adsorbent-assisted physical vapor deposition. J. Adv Funct Mater 2006;16:1985-91. http://dx.doi.org/10.1002/adfm.200600070; b) Qu L, Shi G. Crystalline oligopyrene nanowires with multicolored emission. Chem Commun 2004:2800-1. http://dx.doi.org/10.1039/B412638F.
13. Ishii Y, Omori K, Satozono S, Fukuda M. Dye-doped submicron fiber waveguides composed of hole- and electron-transport materials. Org Electron Physics Mater Appl 2017;41:215–20. http://dx.doi.org/10.1016/j.orgel.2016.11.007.
14. Liao Q, Fu H, Yao. Waveguide modulator by energy remote relay from binary organic crystalline microtubes. J. Adv Mater 2009;21:4153–7. http://dx.doi.org/10.1002/adma.200900997.
15. Li ZZ, Liang F, Zhuo MP, Shi YL, Wang XD, Liao LS. White-Emissive Self-Assembled Organic Microcrystals. Small 2017;13:1–6. http://dx.doi.org/10.1002/smll.201604110.
16. Zhang J, Wang J, Xu X, Chen S, Zhang Q, Yao C, Zhuang X, Pan A, Li L. An air-stable microwire radial heterojunction with high photoconductivity based on a new building block. J Mater Chem C 2015;3:5933–9. http://dx.doi.org/10.1039/C5TC01050K.
17. a) D'Andrade BW, Forrest SR. White organic light-emitting devices for solid-state lighting. Adv Mater 2004;16:1585-95. http://dx.doi.org/10.1002/adma.200400684; b) Kubo Y, Nishiyabu R. White-light emissive materials based on dynamic polymerization in supramolecular chemistry. Polymer 2017;128:257-75. http://dx.doi.org/10.1016/j.polymer.2016.12.082; c) Zhao YS, Fu H, Hu H, Peng A, Yang W, Yao. Tunable emission from binary organic one-dimensional nanomaterials: an alternative approach to white-light emission. J Adv Mater 2008;20:79-83. http://dx.doi.org/10.1002/adma.200700542; d) Lei Y, Liao Q, Fu H, Yao J. Orange−blue−orange triblock one-dimensional heterostructures of organic microrods for white-light emission. J Am Chem Soc 2010;132:1742-3. http://dx.doi.org/10.1021/ja9084435.
18. Abbel R, Grenier C, Pouderoijen MJ, Stouwdam JW, Leclêre PELG. White-light emitting hydrogen-bonded supramolecular copolymers based on π-conjugated oligomers. J Am Chem Soc 2009;131:833-44. http://dx.doi.org/10.1021/ja807996y.

19. Vijayakumar C, Praveen VK, Ajayaghost A. RGB emission through controlled donor self-assembly and modulation of excitation energy transfer: a novel strategy to white-light-emitting organogels. Adv Mater 2009;21:2059-63. http://dx.doi.org/10.1002/adma.200802932.
20. a) Cáceres D, Cebrián C, Rodríguez AM, Carrillo JR, Díaz-Ortiz A, Prieto P, Aparicio F, García F, Sánchez L. Optical waveguides from 4-aryl-4H-1,2,4-triazole-based supramolecular structures. Chem Commun 2013;49:621-3. http://dx.doi.org/10.1039/C2CC37381E; b) Pastor MJ, Torres I, Cebrián C, Carrillo JR, Díaz-Ortiz A, Matesanz E, Buendía J, García F, Barberá J, Prieto P, Sánchez L. 4-aryl-3,5-bis(arylethynyl)aryl-4H-1,2,4-triazoles: multitasking skeleton as a self-assembling unit. Chem Eur J 2015;21:1795-802. http://dx.doi.org/10.1002/chem.201404243; c) Torres I, Carrillo JR, Díaz-Ortiz A, Martín R, Gómez MV, Stegemann L, Strassert CA, Orduna J, Buendía J, Greciano EE, Valera JS, Matesanz E, Sánchez L, Prieto P. Self-assembly of T-shape 2H-benzo[d][1,2,3]-triazoles. Optical waveguide and photophysical properties. RSC Adv 2016;6:36544-53. http://dx.doi.org/10.1039/c6ra02473d; d) Torres I, Díaz-Ortiz A, Sánchez L, Orduna J, Blesa MJ, Carrillo JR, Prieto P. Tunable emission in aggregated T-Shaped 2H-Benzo[d][1,2,3]triazoles with waveguide behaviour. Dyes Pigments 2017;142:212-25. http://dx.doi.org/10.1016/j.dyepig.2017.02.048; e) Martín R, Prieto P, Carrillo JR, Torres I, Strassert CA, Soloviova K, Rodríguez AM, Sánchez L, Díaz-Ortiz A. Colored optical waveguides in self-assembled thiadiazole-based materials. Dyes Pigments 2018;151:327-34. http://dx.doi.org/10.1016/j.dyepig.2018.01.001.
21. Torres I, González-Domínguez JM, Díaz-Ortiz A, Romero-Nieto C, Rominger F, Vázquez E, Carrillo JR, Prieto P. Modulation of Waveguide Behaviour of an ICT 2H-Benzo[d][1,2,3]Triazole Derivative with Graphene. Org Electron 2019;68:1-8. http://dx.doi.org/10.1016/j.orgel.2019.01.033.
22. a) Lakowicz JR. Principles of Fluorescence Spectroscopy; Springer Science & Business Media, Germany, 2013; b) Chemla DS, Zyss J. Nonlinear Optical Properties of Organic Molecules and Crystals; Elsevier, The Netherlands, 2001.
23. Martín R, Prieto P, Carrillo JR, Rodríguez AM, de Cózar A, Boj PG, Díaz-García MA, Ramírez MG. Design, synthesis and amplified spontaneous emission of 1,2,5-benzothiadiazole derivatives. J Mater Chem C 2019;7:9996-10007. http://dx.doi.org/10.1039/C9TC03148K.